JBC RESEARCH ARTICLE

Coordinated regulation of the ribosome and proteasome by PRMT1 in the maintenance of neural stemness in cancer cells and neural stem cells

Received for publication, June 23, 2021, and in revised form, September 19, 2021 Published, Papers in Press, October 4, 2021,
https://doi.org/10.1016/j.jbc.2021.101275

Lu Chen[1,2,3], Min Zhang[1,2,3], Lei Fang[3], Xiaoli Yang[1,2,3], Ning Cao[1,2,3], Liyang Xu[2,3], Lihua Shi[2,3], and Ying Cao[1,2,3,*]

From the [1]Research Institute of Nanjing University in Shenzhen, Shenzhen, China; [2]MOE Key Laboratory of Model Animals for Disease Study, Model Animal Research Center, and [3]Jiangsu Key Laboratory of Molecular Medicine of the Medical School, Nanjing University, Nanjing, China

Edited by George DeMartino

Previous studies suggested that cancer cells resemble neural stem/progenitor cells in regulatory network, tumorigenicity, and differentiation potential, and that neural stemness might represent the ground or basal state of differentiation and tumorigenicity. The neural ground state is reflected in the upregulation and enrichment of basic cell machineries and developmental programs, such as cell cycle, ribosomes, proteasomes, and epigenetic factors, in cancers and in embryonic neural or neural stem cells. However, how these machineries are concertedly regulated is unclear. Here, we show that loss of neural stemness in cancer or neural stem cells *via* muscle-like differentiation or neuronal differentiation, respectively, caused downregulation of ribosome and proteasome components and major epigenetic factors, including PRMT1, EZH2, and LSD1. Furthermore, inhibition of PRMT1, an oncoprotein that is enriched in neural cells during embryogenesis, caused neuronal-like differentiation, downregulation of a similar set of proteins downregulated by differentiation, and alteration of subcellular distribution of ribosome and proteasome components. By contrast, PRMT1 overexpression led to an upregulation of these proteins. PRMT1 interacted with these components and protected them from degradation *via* recruitment of the deubiquitinase USP7, also known to promote cancer and enriched in embryonic neural cells, thereby maintaining a high level of epigenetic factors that maintain neural stemness, such as EZH2 and LSD1. Taken together, our data indicate that PRMT1 inhibition resulted in repression of cell tumorigenicity. We conclude that PRMT1 coordinates ribosome and proteasome activity to match the needs for high production and homeostasis of proteins that maintain stemness in cancer and neural stem cells.

Ribosomes and proteasomes are machineries that are required for basic cellular physiology. Ribosomes are responsible for protein translation from mRNAs. In eukaryotic cells, the mature 80S ribosome is composed of the 40S and 60S subunits. In human, the 40S subunit contains 18S ribosomal RNA (rRNA) and 33 ribosomal proteins, such as RPS2, RPS3, RPS3A, RPS4X, RPS5-RPS21, and RPS23-RPS29, *etc.*; while the 60S subunits contains 5S, 5.8S and 28S rRNAs and 47 ribosomal proteins, mainly RPL3-RPL5, RPL7-RPL19, RPL21-RPL24, RPL23A, RPL26-RPL31, *etc.* (1, 2). Some additional proteins are assembled into pre-40S and pre-60S ribosomal subunits in the nucleoplasm and cytoplasm or required for nuclear export of the pre-60S subunit. These include the nuclear chaperone MDN1 (Midasin), an ATPase critical for proper remodeling of pre-60S subunit (3, 4). The major steps of ribosome biogenesis occur in nucleolus. At late stage of maturation, 80S ribosomes are exported to cytoplasm, where they undergo the last step of maturation and start protein synthesis (2). Therefore, ribosomes are essential for cellular survival, growth, and differentiation. An increase in overall protein levels and production of sufficient ribosomes are a prominent characteristic of cell growth (5, 6). Ribosome biogenesis is indispensible for maintaining pluripotency (7). Vice versa, ribosomes exhibit the ability to transdifferentiate human somatic cells into multipotent state (8, 9). These imply the critical roles of ribosomes in early development and cell differentiation.

While protein synthesis is fundamental for normal physiology of a cell, the reverse process, protein degradation is equally important, because unneeded or damaged proteins are detrimental to a cell. Proteasomes are multienzyme complexes responsible for degrading excessive or wrong proteins, in cooperation with ubiquitin. The 26S proteasome (or proteasome) is the major cellular protease, found in the nucleus and cytoplasm of all eukaryotic cells and playing the central role in the ubiquitin-dependent pathway of protein degradation (10–12). The proteasome consists of a 20S core particle that is responsible for catalytic activity and two 19S regulatory particles that recognize ubiquitinated and misfolded proteins. The 20S catalytic core is composed of two α-rings and two β-rings. An α-ring is made up of seven components PSMA1–PSMA7, while a β-ring includes PSMB1–PSMB7. 19S regulatory particle has more complex constituents, including PSMC1–PSMC6, PSMD1–PSMD4, PSMD6–PSMD8, PSMD11–PSMD14, and ADRM1 (10–13). Other regulatory complexes such as the PA28 activator, consisting of PSME1-PSME3,

* For correspondence: Ying Cao, caoying@nju.edu.cn.

associate with and activate the 20S core (10, 12). Proteasomes are fundamental to life process because of its central function in keeping protein homeostasis, a status essential for maintenance of ESC function and relieving cellular aging (11, 14). Particularly, proteasomes play a key role in promoting self-renewal of neural progenitor cells (NPCs) (15).

Protein arginine methylation is a common type of post-translational modification that is catalyzed by either one of the nine protein arginine methyltransferases (PRMT1-PRMT9). PRMT1 is the main epigenetic factor responsible for asymmetrical dimethylation histone H4 at Arg-3 and functions as a transcriptional coactivator. Besides, PRMT1 also methylates nonhistone proteins, thereby modulating many biological processes such as RNA metabolism, genome stability, transcription, and signal transduction (16, 17). Mouse embryos without Prmt1 cannot develop beyond E6.5 (18). Other major epigenetic factors such as EZH2, LSD1, HDAC1, *etc.*, which mediate different types of epigenetic modifications, are essential for embryonic developmental programs. Loss of either of them causes early embryonic lethality. Downregulation of these proteins is required for neuronal differentiation. They regulate neuronal differentiation from neural stem/progenitor cells (NSCs/NPCs) through different mechanisms (19–23).

Cancer cells are characteristic of NSCs because they have neuronal differentiation potential and most cancer promoting genes or genes upregulated in cancer are neural stemness genes or enriched embryonic neural cells (23–25). Moreover, cell tumorigenicity and pluripotent differentiation potential stem from neural stemness, a property that is predetermined by evolutionary advantage (26, 27). Cancer cells are characteristic of fast cell cycle and proliferation, a feature that needs high level of protein production. In agreement, ribosome biogenesis is upregulated in cancer cells and involved in tumorigenesis (2, 6, 28). Enhanced protein synthesis means a higher demand for regulatory machinery maintaining protein homeostasis. Actually, cancer cells show elevated levels of proteasomes and proteasome activity for protein quality control to promote their survival, growth, and metastasis (13, 29–31). Therefore, a concerted regulation of ribosome and proteasome is required for tumorigenesis. PRMT1 and key epigenetic factors, such as EZH2, LSD1, or HDAC1, are also upregulated in various cancer types and promote cancer (17, 32–34). Consistently, expression of genes for ribosome and proteasome proteins and epigenetic factors is enriched in NSCs or embryonic neural cells during vertebrate embryogenesis (24, 35–37). Here, we show the evidence that coordinated regulation of ribosome biogenesis and proteasome by PRMT1 is required for maintenance of neural stemness in both cancer cells and NSCs, which are highly proliferative and need a high protein production and protein homeostasis.

Results

Loss of PRMT1 function leads to neuronal differentiation in both cancer cells and neural stem cells

PRMT1 functions as an oncoprotein or is upregulated in various types of cancers (17, 32, 38–44). It shows strongly enriched expression in embryonic neural cells during early vertebrate embryogenesis (18, 24), suggesting that it might play a role in maintaining neural stemness. Knockdown of PRMT1 with a validated hairpin RNA (shPRMT1) in lung cancer cell line A549 generated a neuron-like phenotype (Fig. 1*A*) with extended neuritic processes. A key proneuronal differentiation protein NEUROD1 and neuronal markers TUBB3 and MAP2 were not detected in control cells (shCtrl), but detected in knockdown cells (Fig. 1*B*) with immunofluorescence (IF). A similar phenotypic change was observed in colorectal cancer cell line SW480 in response to PRMT1 knockdown (Fig. 1*C*). Accordingly, NEUROD1, TUBB3, and MAP2 were not detected in control cells but detected in knockdown cells (Fig. 1*D*). The melanoma cell line A375 assumed a neuronal-like phenotype after knockdown of PRMT1 (Fig. 1*E*). IF demonstrated expression of neuronal markers TUBB3 and NF-L in knockdown cells (Fig. 1*F*). We then tested the effect of Prmt1 on differentiation of primitive neural stem cells (primNSCs) derived from mouse embryonic stem cells (mESCs). mESCs differentiated into primNSCs and formed floating neurospheres in NSC-specific serum-free medium (Fig. 1*G*). In contrast, knockdown cells showed a phenotype of neuronal differentiation (Fig. 1*G*). Expression of Prmt1 and the neural stemness markers Sox2, Nestin, Sox1, and Pax3 was detected in neurospheres (Fig. 1*H*). However, they were lost in Prmt1 knockdown cells (Fig. 1*H*). Neuronal proteins Neurod1, Tubb3, and Map2 were not present in neurospheres. Prmt1 knockdown resulted in expression of these proteins in cells (Fig. 1*H*), indicating neuronal differentiation of primNSCs in response to Prmt1 inhibition. This neuronal-like differentiation effect in cancer cells and NSCs is similar to our previous observations on inhibition of other cancer-promoting factors in cancer cells and NSCs (23, 24). This suggests that PRMT1/Prmt1 functions in conferring or maintaining neural stemness in both cancer cells and NSCs.

Loss of neural stemness via differentiation causes downregulation of basic cellular machineries, and PRMT1 regulates ribosomes and proteasomes

To explore how PRMT1/Prmt1 functions in cancer cells and NSCs, we identified potential PRMT1/Prmt1 interaction proteins using mass spectrometry. In NE-4C cells, an NSC cell line that was derived from cerebral vesicles of mouse E9 embryos, 1246 proteins were identified as putative Prmt1 interaction partners (Table S1). In hepatocellular carcinoma cell line HepG2, 1494 proteins were identified (Table S2). There are 839 putative interaction partners in common (Fig. 2*A*, Tables S1 and S2), suggesting that PRMT1/Prmt1 mediates largely similar regulatory networks in both cell types. The proteins in NE-4C cells are mostly enriched in pathways that underlie basic cellular physiological functions, such as spliceosome, RNA transport, ribosome, proteasome, *etc.* (Fig. 2*B*). In agreement, the most enriched gene ontology (GO) terms for molecular functions are poly(A) RNA and RNA binding, *etc.*, which are associated biological processes of translation, mRNA processing, RNA splicing, *etc.*, that should occur in

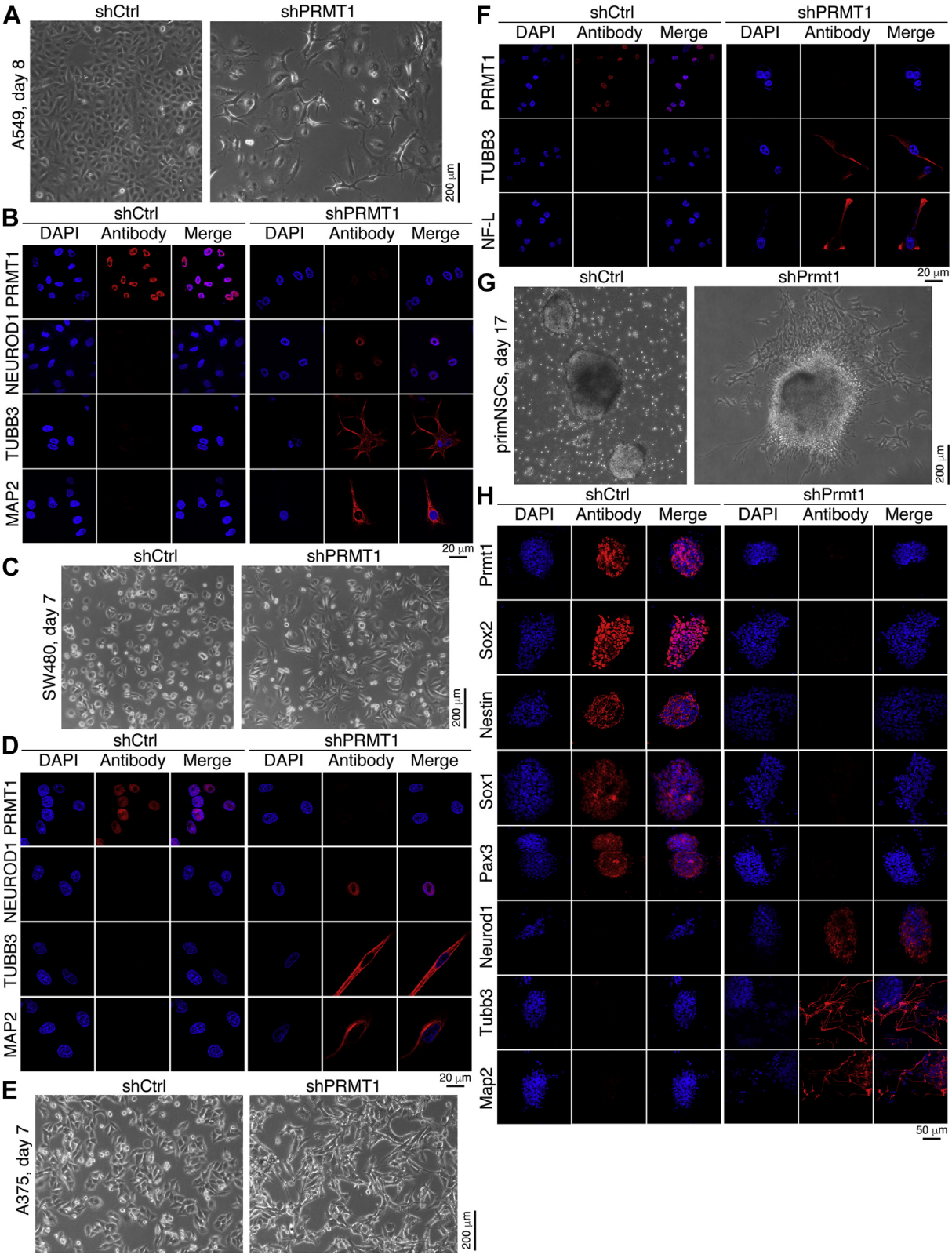

Figure 1. Neuronal differentiation effect induced by knockdown of PRMT1/Prmt1 in cancer cells or NSCs. *A* and *B*, neuronal-like differentiation phenotype by knockdown of PRMT1 (shPRMT1) in A549 cells (*A*), and validation of knockdown effect of PRMT1 and detection of neuronal protein expression (NEUROD1, TUBB3, MAP2) in cells using immunofluorescence (IF) (*B*). Cells infected with lentivirus containing empty vector (shCtrl) were used as control. *C* and *D*, neuronal-like differentiation phenotype by knockdown of PRMT1 in SW480 cells (*C*), and validation of knockdown effect of PRMT1 and detection of neuronal proteins in cells using IF (*D*). *E* and *F*, neuronal-like differentiation effect in A375 cells in response to PRMT1 knockdown (*E*), and validation of knockdown effect of PRMT1 and detection of neuronal markers in cells using IF (*F*). *G*, neurosphere formation of primNSCs derived from mouse ESCs in NSC serum-free medium (*left*) and neuronal differentiation phenotype induced by knockdown of Prmt1 in primNSCs (*right*). *H*, analysis of Prmt1

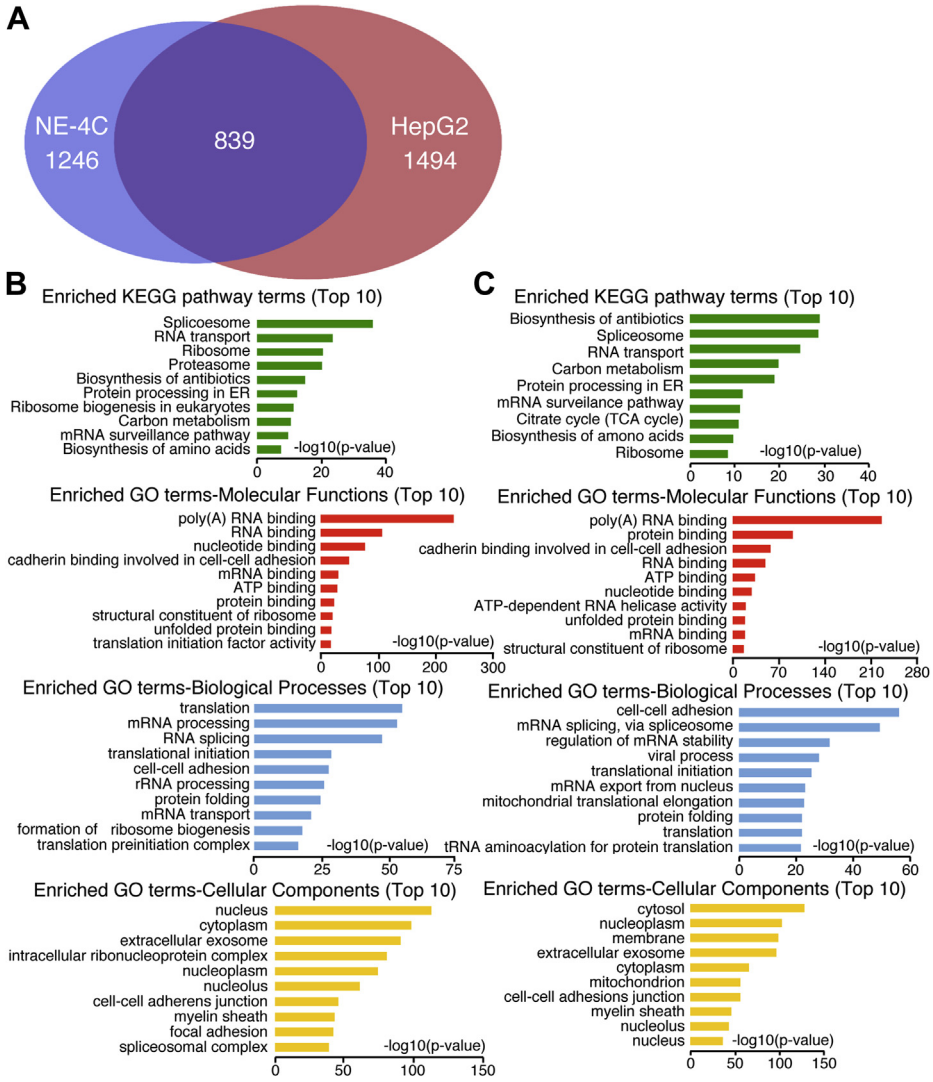

Figure 2. Identification of putative interaction proteins of PRMT1/Prmt1 using mass spectrometry, and bioinformatic analysis on the identified proteins. *A*, a diagram summarizing the number of identified interaction partners of Prmt1/PRMT1 in NE-4C cells and HepG2 cells, and the shared interaction partners between the two cells. *B* and *C*, bioinformatic analysis on enriched pathway and GO terms in the interaction partners in NE-4C (*B*) or HepG2 (*C*) cells.

nucleus and cytoplasm (Fig. 2*B*). The proteins in HepG2 cells are enriched in similar pathways and GO terms (Fig. 2*C*).

Many ribosome and proteasome components were identified as PRMT1/Prmt1 putative interaction partners in the mass spectrometric assays (Tables S1 and S2). Intriguingly, expression of the genes for these components, and the genes for typical epigenetic factors, such as PRMT1, HDAC1, DNMT1, EZH2 and LSD1, is enriched in embryonic neural cells during vertebrate embryogenesis (Fig. S1, *A–C*). Moreover, genes promoting cell cycle are also enriched in embryonic neural cells (Fig. S1*D*). The expression patterns imply that ribosome, proteasome, and the epigenetic factors are required for regulating embryonic neural cells, which represent the basic cell state with fast cell cycle and proliferation. Treatment with retinoic acid (RA), an agent inducing neuronal differentiation from NSCs, caused neuronal differentiation in NE-4C cells (Fig. 3*A*). The differentiation led to a decreased expression in proteasome components such as Psma2, Psmd2, Psmd4, and Adrm1 and ribosome components such as Rps2, Rps3, Rpl24 and Rpl26 (Fig. 3*B*). Decreased proteins also included epigenetic factors Ezh2 and Lsd1 in addition to Prmt1. These are oncoproteins, and Ezh2 and Lsd1 are known to maintain neural stemness (21, 23, 24). Neural stemness proteins Msi1 and Pax6 were decreased and neuronal proteins Nf-l, Tubb3, Map2, and Syn1 were correspondingly upregulated (Fig. 3*B*). Knockdown of Prmt1 also generated a neuronal phenotype in NE-4C cells (Fig. 3*C*). Pax6 was downregulated, but Map2, Nf-l, Syn1, and Tubb3 were upregulated in knockdown cells (Fig. 3*D*). Likewise, the proteasome and ribosome components and epigenetic factors were simultaneously downregulated (Fig. 3*D*). Sox1 and

knockdown effect and detection of neural stemness markers (Sox2, Nestin, Sox1, Pax3) and neuronal proteins (Neurod1, Tubb3, Map2) in neurospheres and in cells with Prmt1 knockdown using IF. In all IF assays, nuclei were counterstained with DAPI.

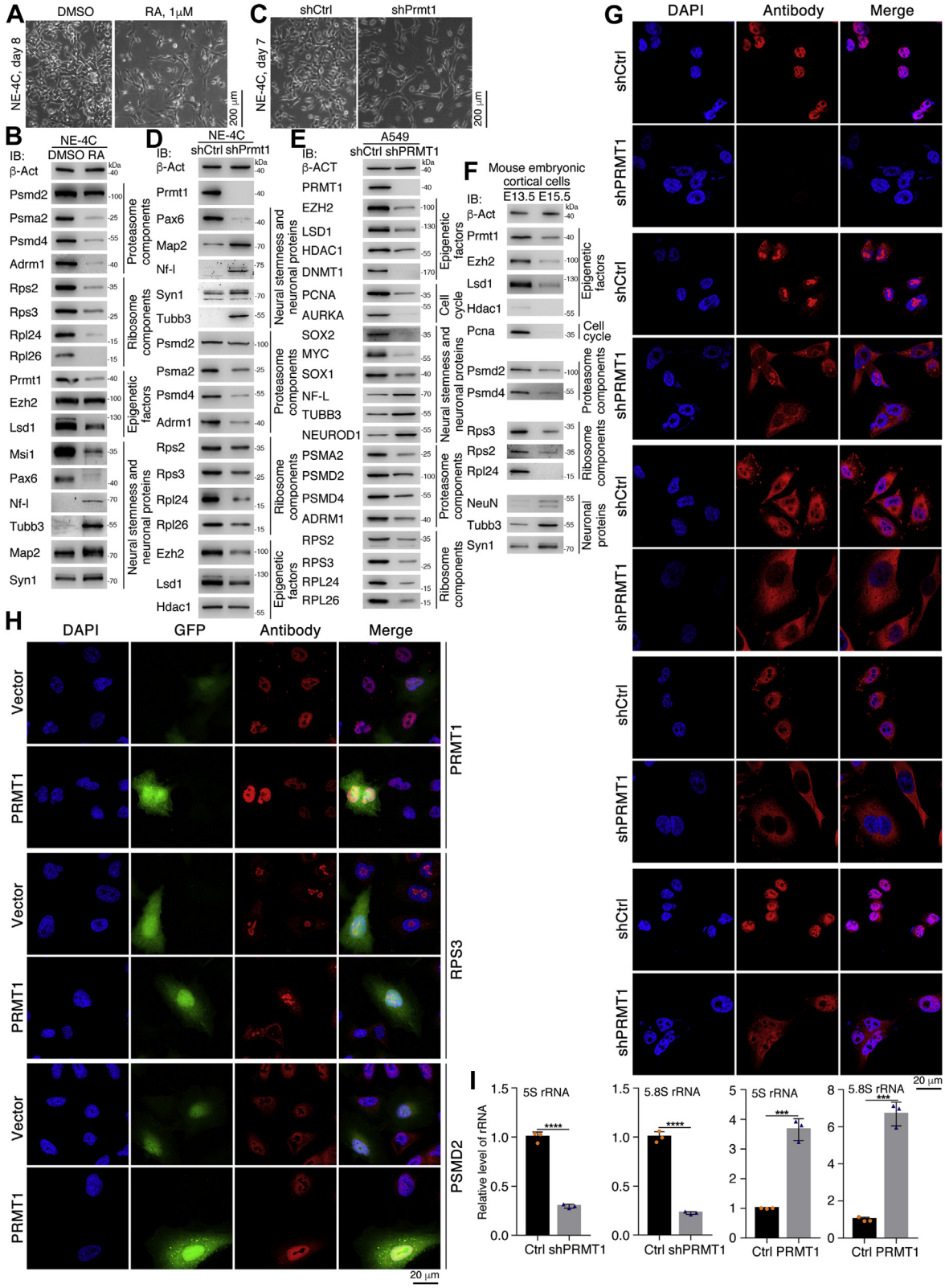

Figure 3. Coordinated regulation of ribosome and proteasome component proteins during neuronal differentiation. *A* and *B*, RA-induced neuronal differentiation phenotype in NE-4C cells shown at the time indicated after treatment (*A*), and immunoblotting (IB) detection of a series of proteasome, ribosome components, epigenetic factors, and neural stemness and neuronal proteins in control cells treated with vehicle (DMSO) and cells treated with RA, as indicated (*B*). *C* and *D*, neuronal differentiation phenotype in NE-4C cells induced by Prmt1 knockdown at the indicated time (*C*), and IB detection of expression of proteins, as indicated, in control (shCtrl) and knockdown (shPrmt1) cells (*D*). *E*, IB detection of various proteins, as indicated, in control A549 (shCtrl) cells and cells with knockdown of PRMT1 (shPRMT1). *F*, IB detection of various proteins, as indicated, in mouse embryonic cortical cells at two developmental stages. *G*, IF detection of the effect of PRMT1 knockdown on the subcellular distribution of ribosome components RPS3 and RPL26, proteasome protein PSMD2 and 20S subunit (20S α + β) in A375 cells. *H*, IF detection of the effect of PRMT1 overexpression on the expression of ribosome and

Pax6, which were expressed in control NE-4C cells, were significantly reduced in cells with knockdown of Prmt1 (Fig. S2*A*). In contrast, Nf-l and Tubb3, which were not expressed in control cells, were expressed in long neurite-like processes in knockdown cells (Fig. S2*B*), supporting again the neuronal differentiation effect. Similar tendency of downregulation of these proteins was observed in A549 cells after PRMT1 knockdown (Fig. 3*E*). Besides, PCNA, AURKA, SOX1/2, and MYC, which promote tumorigenesis, neural stemness, or cell cycle, were reduced. Meanwhile, neuronal proteins NEUROD1, NF-L, and TUBB3 were increased (Fig. 3*E*). The mode of protein expression change in *in vitro* neuronal differentiation resembles what occurs during normal neural development. With the progression of neuronal differentiation in mouse embryos from E13.5 to E15.5, epigenetic factors, the ribosome and proteasome proteins, and cell cycle protein in embryonic cortical cells were reduced, accompanied with an increase in neuronal proteins (Fig. 3*F*). Downregulation of ribosome biogenesis during early forebrain development was reported (45). In addition to reduced protein levels, their cellular localization changes in response to loss of PRMT1. In control A375 cells, RPS3 displayed a ubiquitous distribution in a cell with strong enrichment in nucleoli, the site of ribosome biogenesis. By contrast, it was mainly distributed outside nucleus in cells with PRMT1 knockdown (Fig. 3*G*). In control cells, RPL26 was almost uniformly distributed in both nuclei and cytoplasm except its absence in nucleoli. Nevertheless, it was detected primarily outside the nuclei in knockdown cells (Fig. 3*G*). Proteasome protein PSMD2 is also uniformly expressed in both nuclei and cytoplasm with the absence in nucleoli. Similarly, PRMT1 knockdown caused an exclusively cytoplasmic distribution of PSMD2 (Fig. 3*G*). The 20S proteasomes, which can be recognized by the proteasome 20S α + β antibody (20S α + β), were primarily detected in the nuclei of control cells. In knockdown cells, their distribution was nearly uniform throughout the cells (Fig. 3*G*). Contrary to the effect of knockdown, overexpression of PRMT1 was able to enhance strongly the expression of RPS3 in the nucleoli and the expression of PSMD2 in cell nuclei (Fig. 3*H*). Ribosomal RNAs are essential components of ribosomal assembly and function. 5S and 5.8S rRNA were reduced in response to PRMT1 knockdown and increased when PRMT1 was overexpressed (Fig. 3*I*), an additional indication for that PRMT1 regulates ribosome biogenesis.

MYOD1 is a key factor driving myogenesis and can induce muscle cell-like differentiation in different cancer cells (46). Forced expression of MYOD1 led to the gain of prominent muscle cell phenotype in A375 cells (Fig. 4*A*), concurrent with activation of the muscle cell marker MEF2C, downregulation of proteasome and ribosome proteins and epigenetic factors (Fig. 4*B*). Gain of muscle cell-like phenotype and similar pattern of protein expression change were also observed in A549 cells with forced MYOD1 expression (Fig. 4, *C* and *D*). In control cells expressing GFP, RPS3 was enriched in nucleoli, and GFP did not affect this distribution. However, expression of MYOD1 caused RPS3 to distribute dominantly in cytoplasm, accompanied with the loss of enrichment in nucleoli (Fig. 4*E*). RPL26 was expressed in both nuclei and cytoplasm in control cells; whereas in cells expressing MYOD1, the nuclear fraction of RPL26 expression was reduced, rendering the protein to distribute primarily in cytoplasm. PSMA2 showed expression in both nuclei and cytoplasm, with slightly higher expression in nuclei; MYOD1 caused a reduction of its nuclear expression (Fig. 4*E*). The proteasome 20S subunit (20S α + β) displayed a similar pattern of expression in control cells. In cells expressing MYOD1, it was expressed almost entirely in cytoplasm, with a loss of expression in nuclei (Fig. 4*E*). Therefore, muscle cell differentiation driven by MYOD1 expression led to not only the decrease in overall expression level of ribosome and proteasome components, but also their subcellular distribution, an effect similar to what was observed in neuronal differentiation. Recently, we showed that the myoblast C2C12 cells gained the phenotype of NSCs and hence tumorigenicity when the gene for Myod1 was knocked out (26). Here, we found that the abovementioned epigenetic factors, proteasome and ribosome proteins were upregulated in knockout (KO) cells, as compared with wild-type (WT) C2C12 cells (Fig. 4*F*). Taken together, reduced neural stemness in both NSCs and cancer cells *via* differentiation results in reduced expression and altered subcellular distribution of ribosome and proteasome components and a series of epigenetic factors in a coordinated manner. Vice versa, gain of neural stemness leads to an opposite change. Therefore, enrichment of basic machineries is an intrinsic feature of neural stemness, and PRMT1 might play a role in the coordination of these basic machineries.

PRMT1 mediates ribosome and proteasome protein stability via *interaction with USP7*

Protein coimmunoprecipitation (Co-IP) confirmed that PRMT1 interacted with EZH2, LSD1, and HDAC1, the proteasome components PSMD2, PSMD4, PSMA2, and ADRM1, and the ribosome components RPS3, RPL24, and RPL26 (Fig. 5*A*). In A375 cells with PRMT1 knockdown, gene expression for epigenetic factors except DNMT1, ribosome and proteasome component proteins were mostly not significantly affected (Fig. S3*A*). Nevertheless, there was a general tendency of upregulation of neuronal genes and downregulation of neural stemness genes, in agreement with neuronal-like differentiation phenotype. Similar patterns of gene expression change were found in A549 cells after PRMT1 knockdown (Fig. S3*B*). Therefore, PRMT1 should regulate the protein expression at posttranscriptional level. Indeed,

proteasome proteins in A549 cells. Cells infected with the virus containing only the vector (Vector) as a control. *I*, detection of the change in 5S and 5.8S rRNA in A549 cells with PRMT1 knockdown or overexpression using RT-qPCR. Significance in change of rRNA levels was calculated for experiments in triplicate using unpaired Student's *t* test. Data are shown as mean ± SD. ***$p < 0.001$, ****$p < 0.0001$.

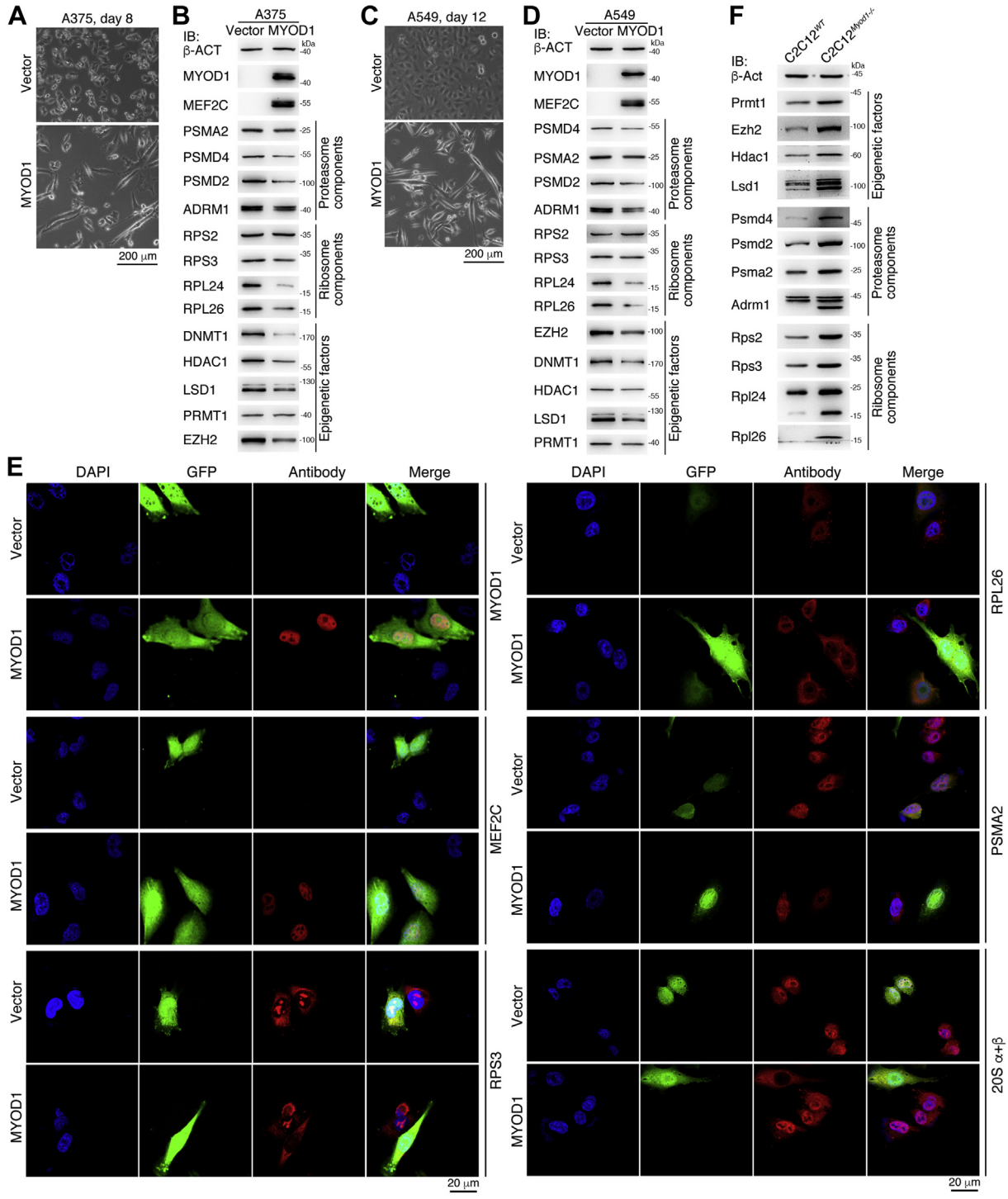

Figure 4. Effect of MYOD1-induced differentiation on the expression of ribosome and proteasome components and epigenetic factors. *A*, phenotypic change in A375 cells infected with virus containing MYOD1. Cells infected with virus containing the empty vector were used as a control. *B*, IB detection of expression change of a series of proteins, as indicated, in control A375 cells and cells with forced MYOD1 expression. *C*, phenotypic change in A549 cells in response to MYOD1 expression. *D*, detection of protein expression, as indicated, in control cells and cells with MYOD1 expression using IB. *E*, IF detection of expression and subcellular distribution of a muscle cell marker, ribosome and proteasome proteins, and the proteasome 20S subunit in control cells and cells with MYOD1 expression. *F*, expression alteration in a series of proteins, as indicated, in wild-type C2C12 ($C2C12^{WT}$) cells and the cells with knockout of *Myod1* gene ($C2C12^{Myod1-/-}$).

inhibition of PRMT1 resulted in an enhanced ubiquitination of RPS3, RPL26, and PSMD2, ultimately leading to their degradation (Fig. 5*B*). Among the putative interaction partners of PRMT1/Prmt1 are deubiquitinating enzymes, USP5, USP7, USP10, and USP14 (Tables S1 and S2), which are involved in protein deubiquitination. USP7 is a well-characterized deubiquitinase and oncoprotein, the gene of which shows enriched transcription in embryonic neural cells (24). USP7 interacted with PSMD2, PSMD4, RPS3, and RPL26, in addition to PRMT1 (Fig. 5*C*). In either A549 or A375 cells, knockdown of

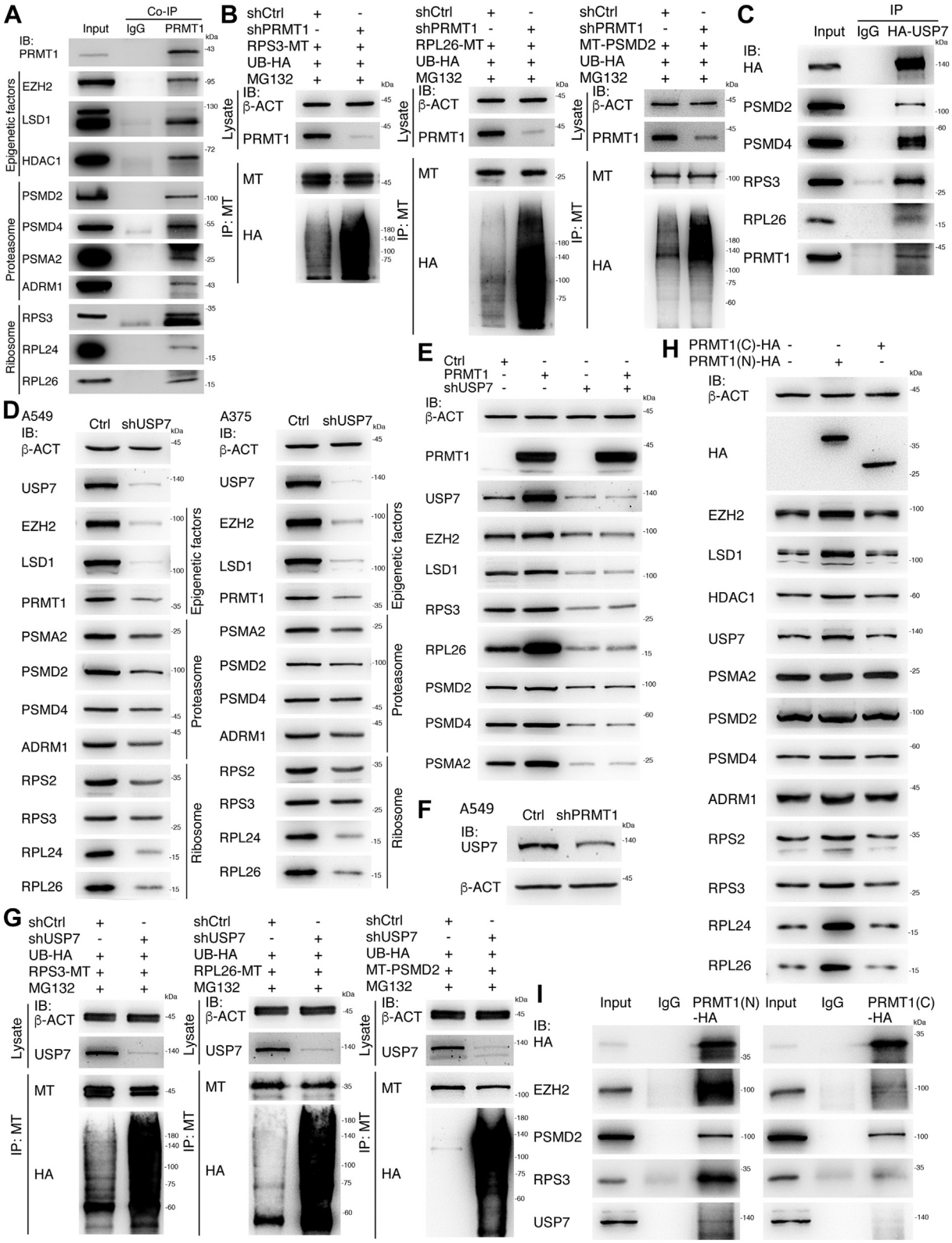

Figure 5. Regulation of ribosome, proteasome component proteins, and epigenetic factors by PRMT1. *A*, Co-IP confirmation of interaction between PRMT1 and a series of epigenetic factors, ribosome and proteasome proteins and a neural stemness protein, which were identified in mass spectrometry. *B*, ubiquitination of overexpressed RPS3, RPL26, and PSMD2, and the effect of PRMT1 knockdown on the ubiquitination of these proteins. *C*, interaction of USP7 with ribosome and proteasome proteins and PRMT1. *D*, IB detection of USP7 knockdown on the expression of proteins as indicated, in A549 and A375 cells. *E*, dependence of PRMT1-mediated protein expression on USP7. *F*, effect of PRMT1 knockdown on USP7 expression. *G*, the effect of USP7 knockdown on the ubiquitination of overexpressed RPS3, RPL26, and PSMD2. *H*, forced expression of PRMT1(N) and PRMT1(C) on the expression of proteins. *I*, differential interaction of PRMT1(N) and PRMT1(C) with proteins.

USP7 using a validated short-hairpin RNA (shUSP7) (23) led to downregulation of epigenetic factors, proteasome and ribosome proteins (Fig. 5*D*). PRMT1 overexpression caused an increment in USP7, EZH2, LSD1, ribosome and proteasome proteins (Fig. 5*E*). Similar to PRMT1 knockdown, inhibition of USP7 led to downregulation of these proteins. However, PRMT1 overexpression could not reverse the decreased protein expression when USP7 was simultaneously inhibited (Fig. 5*E*), indicating that PRMT1-mediated protein expression is dependent on USP7 activity. Similar to ribosome and proteasome proteins, USP7 was also downregulated when PRMT1 was knockdown (Fig. 5*F*). Furthermore, RPS3, RPL26, and PSMD2 were heavily ubiquitinated when USP7 was blocked (Fig. 5*G*), indicating that USP7 has a direct influence on the ubiquitination of its interaction partners. We split PRMT1 into N-terminal (1–200 aa) and C-terminal (201–371 aa) parts, designated as PRMT1(N) and PRMT1(C), respectively. Forced expression of PRMT1(N) in cells could still enhance the expression of epigenetic factors, proteasome and ribosome proteins, and USP7, but less strongly than the WT protein; whereas PRMT1(C) could not (Fig. 5*H*). Correspondingly, PRMT1(N) showed more significant interactions with its interaction partners than PRMT1(C) (Fig. 5*I*). Therefore, the N-terminal part, which contains SAM or AdoMet-MTase domain (92–192 aa), is responsible for PRMT1-mediated protein stability. In summary, PRMT1 regulates the stability of ribosome and proteasome proteins *via* interaction with USP7.

The ribosome and proteasome activity regulates EZH2, LSD1, and HDAC1, which maintains neural stemness

PRMT1 knockdown inhibits both ribosome biogenesis and proteasome assembly, thereby disrupting their functions. We further tested the effect of specific inhibition of ribosomal function on protein expression. MDN1 is required for maturation and nuclear export of pre-60S ribosome subunit (47). In cells overexpressing PRMT1, the epigenetic factors, proteasome and ribosome component proteins were upregulated (Fig. 6*A*). When MDN1 was knocked down, most of these proteins were downregulated. If PRMT1 was added to cells with MDN1 inhibition, expression level of the downregulated proteins was increased again (Fig. 6*A*). These data demonstrate that disruption of ribosome activity causes a reduced expression of these proteins, which can be reversed by PRMT1-mediated protein stabilization.

EZH2, LSD1, and HDAC1 are involved in maintaining neural stemness (19–23). In addition to that disrupted ribosome biogenesis causes reduced expression of these factors, they showed an accelerated degradation in cells with PRMT1 inhibition, as compared with the proteins in control cells in a time-course analysis (Fig. 6, *B* and *C*), and also showed an enhanced ubiquitination in response to PRMT1 inhibition (Fig. 6, *D* and *E*). This means that, without *de novo* protein synthesis, EZH2, LSD1, and HDAC1 degrade rapidly, reinforcing that the machineries for protein synthesis and degradation must be maintained in a balance. IF also revealed an enhanced expression of EZH2, LSD1, and HDAC1 in cells overexpressing PRMT1 (Fig. 6*F*).

Reduction of EZH2, LSD1, or HDAC1 causes neuronal differentiation. We examined how PRMT1 influenced neuronal differentiation by focusing on EZH2, because its target genes during neuronal differentiation were characterized. EZH2 regulates transcription of neuronal genes such as *NEUROD1* and *TUBB3*, *via* binding to promoters of these genes (23). PRMT1 knockdown caused a decreased binding of EZH2 to different regions of *TUBB3* and *NEUROD1* promoters (Fig. 6*G*), EZH2 is the key enzyme catalyzing trimethylation of lysine 27 of histone H3 (H3K37me3), an epigenetic marker for transcriptional repression. Correspondingly, H3K27me3 was reduced in different promoter regions of *TUBB3* and *NEUROD1*. By contrast, the epigenetic marker H3K4me3 for transcriptional activation was increased in different promoter regions of *TUBB3* and *NEUROD1* in response to PRMT1 knockdown (Fig. 6*G*). Therefore, knockdown of PRMT1 in cells led to decreased expression of EZH2, causing a change in H3K37me3 and H3K4me3 marks in bivalent promoters and establishing a state for transcription of these genes during differentiation.

Inhibition of PRMT1 inhibits malignant features and tumorigenicity of cancer cells and NSCs

Since the epigenetic factors, ribosome biogenesis, and proteasome play cancer-promoting roles, their inhibition should generate a suppression effect on malignant features and tumorigenicity. Fast cell cycle and proliferation are a typical feature of cancer cells. A transcriptomic analysis demonstrated that PRMT1 knockdown in A549 cells led to a general transcriptional change that is mostly associated with cell cycle, mitotic nuclear division, chromosome, protein binding, *etc.*, according to GO, and with cell cycle, DNA replication according to pathway classifications (Fig. S4*A*). This is coherent with the neuronal-like differentiation effect induced by inhibition of PRMT1 (Fig. 1*A*). Furthermore, PRMT1 knockdown strongly inhibited the capability of invasion and migration in A549, A375, and NE-4C cells (Fig. S4, *B*, *E* and *H*). Meanwhile, compared with control cells, knockdown cells were unable to form large colonies in soft agar (Fig. S4, *C*, *D*, *F*, *G*, *I* and *J*), an indication of inhibited cell proliferation and growth. Then we tested how the tumorigenic potential was affected in the knockdown cells. A375 cells formed xenograft tumors in nude mice. However, knockdown of PRMT1 in the cells abolished the tumorigenicity of A375 cells, because no tumors formed by the knockdown cells (Fig. 7, *A*–*C*). NE-4C cells formed tumors in all injected mice, as we reported recently (26), Prmt1 knockdown severely compromised its tumorigenic potential (Fig. 7, *D*–*F*). We compared gene expression representing different cell differentiation between the tumors derived from control NE-4C cells and the tumors derived from knockdown cells. There was a general tendency that expression of genes representing neural stemness (Fig. 7*G*) and genes representing neuronal differentiation (Fig. 7*H*) was lower in knockdown tumors than control tumors. Moreover, genes denoting

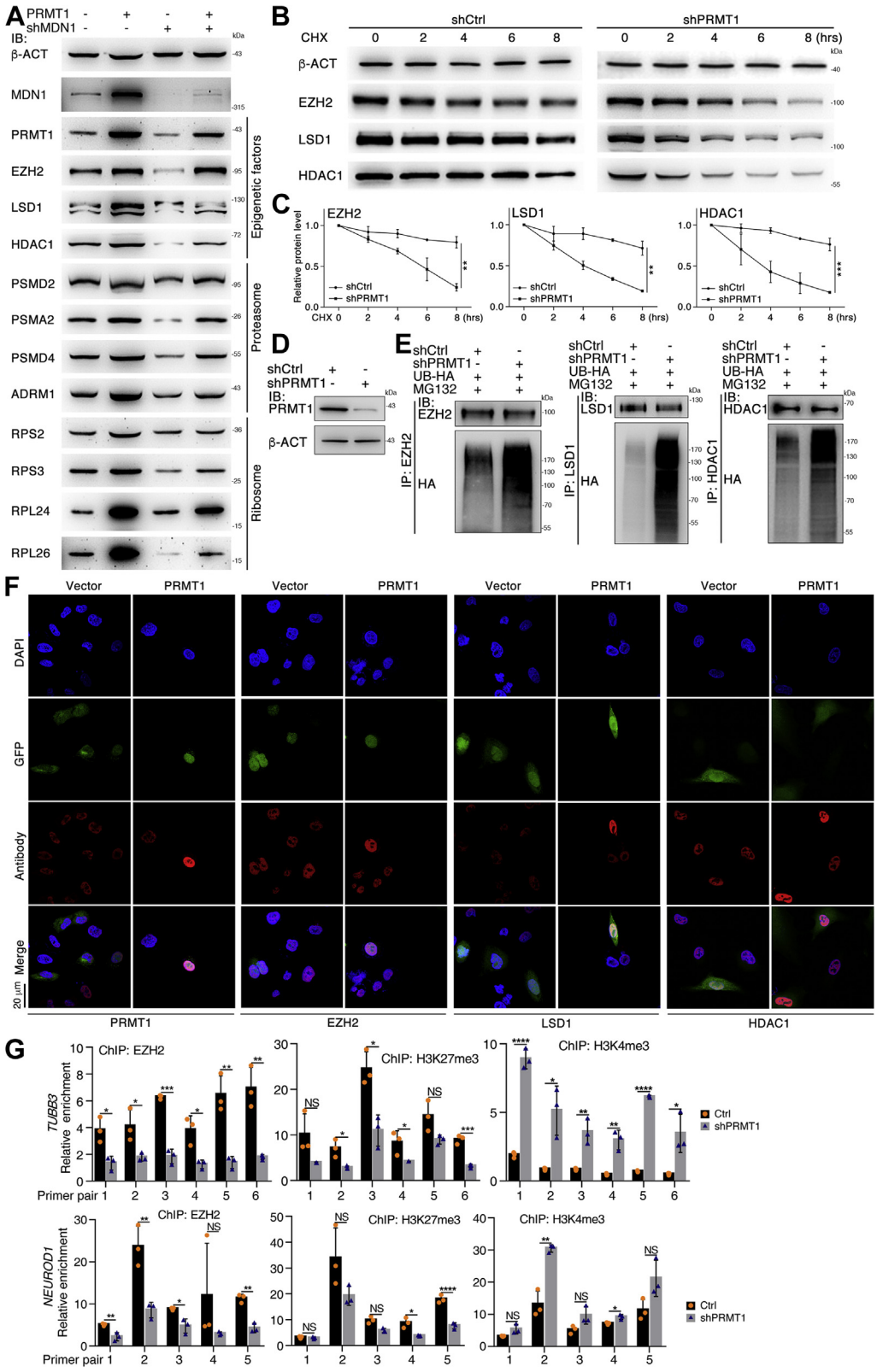

Figure 6. Regulatory effect of ribosome and proteasome on expression of proteins that maintain neural stemness. *A*, IB detection of the repressed expression of proteins by specific disruption of ribosome activity, and the rescue effect by PRMT1 in A549 cells. *B*, analysis of the effect of protein degradation in response to inhibition of *de novo* protein synthesis *via* CHX treatment of HEK293T cells in a time series and PRMT1 knockdown. *C*, quantification of relative protein levels in triplicate experiments as in (*B*). Significance in difference of protein level was calculated using unpaired Student's *t* test. Data are shown as the mean ± SD. $^{**}p < 0.01$, $^{***}p < 0.001$. *D* and *E*, analysis of the effect of protein ubiquitination in response to PRMT1 knockdown. Control cells or cells with PRMT1 knockdown were overexpressed with HA-tagged Ubiquitin (UB-HA) and treated with MG132. Ubiquitination of EZH2, LSD1, and HDAC1 in control cells and knockdown cells was detected with immunoprecipitated proteins with their respective antibodies. *D*, displays PRMT1 knockdown efficiency in the cells. *F*, IF detection of the effect of PRMT1 overexpression on the expression of EZH2, LSD1, and HDAC1 in A549 cells. Nuclei

endodermal tissue differentiation (*Afp*, *Gata4*, *Sox17*) and epithelial cells (*Cdh1*) were significantly upregulated, whereas the genes for mesodermal tissue differentiation (*Desmin*, *Myh4*, *Acta2*, *Myog*) were downregulated in knockdown tumors (Fig. 7*I*). There was a reduction in the expression of the epigenetic factors and the components of the proteasome and ribosome in knockdown tumors (Fig. 7*J*). Our previous study and the study from other groups demonstrated that tumorigenicity and pluripotent differentiation potential is derived from neural stemness (26, 48, 49). PRMT1/Prmt1 knockdown causes a neuronal differentiation effect and thus loss or reduced neural stemness in cancer cells or NSCs, it is coherent that knockdown cells show a loss of or reduced tumorigenicity. Additionally, tissue or cell differentiation in tumors from NE-4C knockdown cells was compromised as compared with differentiation in tumors from control cells. Knockdown tumors show a differentiation bias toward endodermal tissues but ectodermal (neural) and mesodermal differentiation was both undermined. In summary, PRMT1 maintains the stability of ribosome and proteasome proteins *via* interaction with USP7, thereby keeping a high level of production of proteins for maintaining neural stemness and protein homeostasis in neural stem or cancer cells, *i.e.*, tumorigenic cells. Differentiation will cause a reduction of these proteins and a loss of neural stemness, consequently leading to a loss of tumorigenicity (Fig. 7*K*).

Discussion

Cancer cells are characteristic of NSCs because both cell types are tumorigenic and share similar regulatory networks (23, 24, 26), and both have pluripotent differentiation potential (26, 27, 48, 49). The link between neural stemness, tumorigenicity, and differentiation potential is envisaged by the "neural default model" of embryonic pluripotent cells, which means the default fate of embryonic pluripotent cells is neural (49–52). Meanwhile, ESCs are tumorigenic, similar to embryonic carcinoma cells. In a general sense, neural stemness underlies two coupled cell properties, tumorigenicity and differentiation potential (26). Ribosomes, proteasomes, and epigenetic modification factors are usually considered to be not cell-type-specific. However, the genes for the machineries for basic cellular physiological functions and developmental programs, such as cell cycle, ribosome biogenesis, proteasome assembly, epigenetic modification, *etc.*, are mostly enriched in embryonic neural cells (Fig. S1). These machineries work together to establish the property of neural stemness, a basal and most proliferative state. A highly proliferative state needs high activity of both ribosomes and proteasomes, and low activity of these machineries fits for a low or nonproliferative state. This needs a coordination to achieve such a balance. The coordination is reflected by their enrichment in embryonic neural cells, and by that these factors are upregulated in and promote cancers. When either NSCs or cancer cells differentiate into neuronal or neuronal-like cells, PRMT1, ribosomal, and proteasomal components are downregulated. Meanwhile, EZH2, LSD1, and HDAC1, *etc.*, are reduced. In embryos, expression of these proteins is decreased with the progression of neural development ((45), present study). Differentiation into muscle-like cells causes the same tendency of expression change, which mimics the difference in gene expression levels between neural and nonneural cells in early embryos (Fig. S1). Differentiation of ESCs, whose default fate is primNSCs, is accompanied with downregulation of the proteasome component PSMD11. It is thus deduced that cleanup is necessary for maintaining pluripotency (12). Our suggestion is that a high level of proteasome activity is required for matching high protein production in a highly proliferative state. By contrast, dedifferentiation by loss of Myod1 in myoblast cells leads to the gain of the property of neural stemness and tumorigenicity (26). Coherently, the epigenetic factors and the ribosome and proteasome components are upregulated. Taking together, neural stemness, representing a basal and highly proliferative state, is defined by a high level of the machineries required for basic cell physiological functions. Upon differentiation, these machineries are decreased; and loss of neural stemness leads to loss of or reduced tumorigenicity in cancer cells ((24, 26), present study). Reversal of the differentiated state, like that occurs during tumorigenesis, restores a high level of these machineries again.

It needs a coordination mechanism to achieve a balanced level of different machineries. PRMT1 might play such a role. PRMT1 interacts not only with ribosome and proteasome components, but also with deubiquitinases, such as USP7, which promote protein stability. PRMT1 bridges deubiquitinases to ribosome or proteasome proteins and stabilize these proteins. In the presence of a high level of PRMT1 expression, a high level of ribosome and proteasome activity is maintained, hence generating high expression of proteins that maintain neural stemness and tumorigenicity, such as EZH2, LSD1, HDAC1, *etc.* Reduced PRMT1 causes an opposite effect, leading to a reduced level of neural stemness proteins, stimulation of differentiation genes, and reduced tumorigenicity. Ribosome biogenesis starts in the nucleolus, progresses to the nucleoplasm, and matures and functions in the cytoplasm. In tumorigenic cells with fast proliferation, the primary distribution of PRMT1, ribosome and proteasome proteins is in cell nucleus. USP7 is also mainly distributed in nucleus and promotes the maintenance of neural stemness (53). When differentiation occurs, such as muscle-like differentiation or neuronal differentiation, cell cycle and proliferation slow down. Expression level of these proteins is decreased, with the change in the distribution from mainly in nucleus to

were counterstained with DAPI. *G*, influence of PRMT1 knockdown on the binding of EZH2 to *TUBB3* and *NEUROD1* promoters, and on the change in H3K27me3 and H3K4me3 in these promoters. In control (Ctrl) or knockdown A375 cells, chromatin fragments were precipitated with antibodies against EZH2, H3K27me3, and H3K4me3, respectively, and detected with qPCR using primers amplifying different regions of promoters. Significance in difference in amplified promoter fragments was calculated using unpaired Student's *t* test based on experiments in triplicate. Data are shown as the mean ± SD. $*p < 0.05$, $**p < 0.01$, $***p < 0.001$, $****p < 0.0001$. NS, not significant.

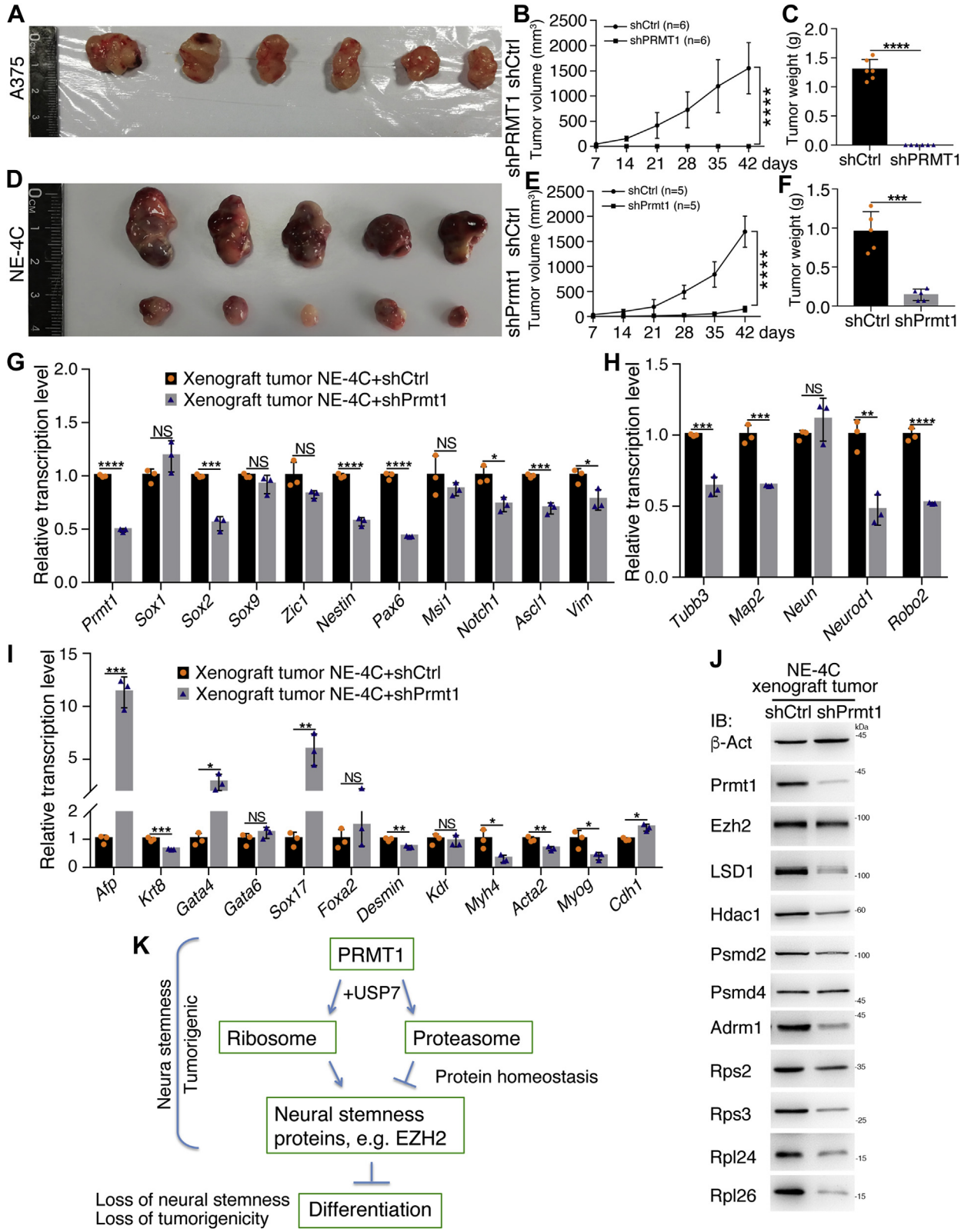

Figure 7. Suppression effect of PRMT1/Prmt1 knockdown on cell tumorigenicity. *A–C*, tumor formation of control (shCtrl) and knockdown (shPRMT1) A375 cells in each six injected nude mice (*A*), and difference in tumor volume (*B*) and weight (*C*) between the two groups. *D–F*, tumor formation of control (shCtrl) and knockdown (shPrmt1) NE-4C cells in each five injected nude mice (*D*), and difference in tumor volume (*E*) and weight (*F*) between the two groups. In (*B*) and (*E*), significance of difference in tumor volume between two groups of mice was calculated using two-way ANOVA-Bonferroni/Dunn test. In (*C*) and (*F*), significance of difference in tumor weight was calculated using unpaired Student's *t* test. Data are shown as the mean ± SD. ***$p < 0.001$, ****$p < 0.0001$. *G–I*, comparison of expression of genes representing neural stemness (*G*), neuronal differentiation (*H*), and mesodermal and endodermal differentiation (*I*) between xenograft tumors derived from control NE-4C cells (NE-4C+shCtrl) and tumors from NE-4C knockdown cells (NE-4C+shPrmt1), as detected with RT-qPCR. Significance in expression change was calculated for experiments in triplicate using unpaired Student's *t* test. Data are shown as the

cytoplasm. Therefore, expression and distribution of these proteins are concertedly regulated to match the proliferation or differentiation status. Besides PRMT1 regulation of ribosome biogenesis *via* promoting RPS3 and RPL26 stability, ribosome biogenesis is more extensively tuned by different PRMTs (54–58). Regulation of proteasome assembly by PRMTs has not been reported.

The roles of PRMT1 are not limited to the regulation of ribosome biogenesis and proteasome assembly. Our mass spectrometric assay also identified the components of the machineries for spliceosome and translation initiation, *etc.*, as putative interaction partners of PRMT1, suggesting that it might function more extensively in the regulation of basic cellular physiological processes. In fact, loss of PRMT1 causes decreased arginine methylation of the translation initiation complex, leading to a defect of its assembly and translation and consequently, a repression effect on cancer cells (59). The association between PRMTs, including PRMT1, and RNA splicing was also investigated (60, 61). Hence, PRMT1 is involved in the coordination of basic cell physiological machineries, which work together to define a basal and highly proliferative property in either NSCs or cancer cells.

Experimental procedures

Cell culture

C57BL/6 mESCs, NE-4C, SW480, A375, HepG2, HEK293T, C2C12^{WT}, and C2C12$^{Myod1-/-}$ cells were obtained and cultured exactly as described (23, 26). A549 (Cellbank of Chinese Academy of Sciences, #TCHu150) was cultured in F-12K medium (Thermo Fisher Scientific, #21127022). Cancer cell lines were authenticated with short tandem repeat profiling, and cells were detected free of *mycoplasma* contamination with PCR.

Immunofluorescence

Immunofluorescence was performed using conventional method as described (25). Primary antibodies were EZH2 (Cell Signaling Technology, #5246), HDAC1 (Cell Signaling Technology, #5356), LSD1 (Cell Signaling Technology, #2139), MAP2 (Abcam, #ab183830), MEF2C (Cell Signaling Technology, #5030), MYOD1 (Novus Biologicals, #NB100-56511), NESTIN (R&D systems, #AF2736), NEUROD1 (Cell Signaling Technology, #4373), NF-L (Cell Signaling Technology, #2837), PAX6 (Abcam, #ab195045), PRMT1 (Cell Signaling Technology, #2449), PSMA2 (Abclonal, #A2504), PSMD2 (Abclonal, #A1999), RPL26 (Abclonal, #A16680), RPS3 (Abclonal, #A2533), SOX1 (Abcam, #ab109290), SOX2 (Cell Signaling Technology, #23064), TUBB3 (Cell Signaling Technology, #5568), 20S α + β (Abcam, #ab22673). Secondary antibodies were anti-mouse IgG (FITC-conjugated) (Sigma-Aldrich, #F9137), anti-mouse or rabbit Alexa Flour 594 (Thermo Fisher Scientific, #A21207, #A21203). Cell nuclei were counterstained with DAPI. After staining, slides were washed and mounted with SlowFade Gold Antifade Mountant (Thermo Fisher, #S36936). Cells were viewed and photographed with a fluorescence microscope (Zeiss LSM 880).

In vitro *neural differentiation of mESCs and chemical treatment of cells*

Primitive NSCs (primNSCs) were differentiated from mESCs by culturing mESCs in defined serum-free NSC medium Ndiff227 (Takara, #Y40002) at 37 °C with 5% CO_2. PrimNSCs formed free-floating neurospheres in the medium 4 days later and the neurospheres grew larger with continuing culture. WT or cells with PRMT1/Prmt1 knockdown were also cultured in this medium to test their ability in neurosphere formation and neuronal differentiation effect. To induce neuronal differentiation in NE-4C cells, retinoic acid (RA. Sigma-Aldrich, #R2625) was added to the culture medium to a final concentration of 1 μM for 24 h. Later on, RA was removed and cells were cultured further till significant differentiation occurred, as indicated in the text. HEK293T cells were treated with MG132 (Selleckchem, #S2619) at 25 μM for 18 h to detect protein ubiquitination, and A375 cells were treated with MG132 at 25 μM for 18 h for the detection of protein expression. To examine protein half-life, HEK293T cells that were infected with control virus (shCtrl) or PRMT1 knockdown (shPRMT1) virus were treated with cycloheximide (CHX. Selleckchem, #S7418) at a final concentration of 50 μg/ml in a time series of 0, 2, 4, 6, and 8 h, respectively.

Immmunoblotting (IB)

Whole cell lysates (WCLs) were prepared, and IB detection of protein expression in cells was carried out using conventional methods. Blots were developed with a Western blotting substrate (Tanon, #180-501). Primary antibodies were: β-Act (Cell Signaling Technology, #4970), ADRM1 (Abclonal, #A4481), AURKA (Cell Signaling Technology, #14475), DNMT1 (Abcam, #ab13537), EZH2 (Cell Signaling Technology, #5246), HDAC1 (Cell Signaling Technology, #5356), LSD1 (Cell Signaling Technology, #2139), MAP2 (Abcam, #ab183830), MEF2C (Cell Signaling Technology, #5030), MSI1 (BioLegend, #869101), MYC (Abcam, #ab32072), MYOD1 (Novus Biologicals, #NB100-56511), NEUROD1 (Cell Signaling Technology, #4373), NF-L (Cell Signaling Technology, #2837), PAX6 (Abcam, #ab195045), PCNA (Cell Signaling Technology, #13110), PRMT1 (Cell Signaling Technology, #2449), PSMA2 (Abclonal, #A2504), PSMD2 (Abclonal, #A1999), PSMD4 (Abcam, #ab137109), RPL24 (Abclonal, #A14255), RPL26 (Abclonal, #A16680), RPS2 (Abclonal, #A6728), RPS3 (Abclonal, #A2533), SOX1 (Abcam, #ab109290), SOX2 (Cell Signaling Technology, #23064), SYN1 (Cell Signaling Technology, #5297), TUBB3 (Cell Signaling Technology, #5568), USP7

mean ± SD. *$p < 0.05$, **$p < 0.01$, ***$p < 0.001$, ****$p < 0.0001$. *J*, protein expression difference between tumors from control NE-4C cells and tumors from knockdown cells. Pooled protein samples of the control and knockdown groups, respectively, were used for IB. *K*, a model depicting the coordinated regulation of ribosome and proteasome by PRMT1 in the maintenance of neural stemness, the basic cell state of fast cell cycle, and proliferation. NS, not significant.

(Abclonal, #A3448), HA-tag (Cell Signaling Technology, #3724), and Myc-tag (Abclonal, #AE010). The secondary antibodies were HRP-conjugated goat anti-rabbit or anti-mouse IgG (Sangon Biotech, #D110058; #D110087). Blotting signals in the experiment of time-course treatment of cells with CHX were quantified with ImageJ software (https://imagej.nih.gov/).

Plasmid construction, viral production, cell infection or transfection

For functional knockdown of PRMT1/Prmt1 and MDN1, an shRNA-based approach was used. The sequences of shRNAs against human PRMT1, MDN1, USP7, and mouse Prmt1 were the validated MISSION shRNAs (Sigma-Aldrich). The shRNAs were TRCN0000290479 (human *PRMT1*), TRCN0000018491 (mouse *Prmt1*), TRCN0000229952 (human *MDN1*), and TRCN0000004058 (human *USP7*), and subcloned to the lentiviral vector pLKO.1. For transient overexpression of human RPS3, RPL26, PSMD2, and USP7, the open reading frames (ORFs) were subcloned to pCS2+4×HAmcs or pCS2+6×MTmcs vectors. For overexpression of PRMT1 or MYOD1, the ORFs were subcloned to pLVX-IRES-puro and pLVX-IRES-ZsGreen lentiviral vectors. Complete PRMT1 ORF and the coding region for aa 1 to 200 and for aa 201 to 371 were also subcloned to pCS2+4×HAmcs or pCS2+6×MTmcs vector for the use of transient overexpression.

Viral production and cell infection were performed essentially as described (23). For stable knockdown or overexpression assays, virus packaging plasmids and shRNA or overexpression constructs were transfected into HEK293T cells using polyethylenimine (PEI). Polybrene at a final concentration of 10 μg/ml was added to the lentiviral supernatant 48 h after transfection. The supernatant was centrifuged at 4 °C to concentrate the lentiviral particles, which were used for infecting cells. Forty-eight hours after infection, cells were selected with puromycin at 2 μg/ml in culture for 3 days when a puromycin selection vector was used. Cells were cultured further until a desired time when a significant phenotypic change was observed, or they were harvested for additional assays. Virus packaging with the empty vector and cell infection with the virus were performed in parallel, which was used as a negative control for knockdown or overexpression assay, respectively.

For transient overexpression assays, HEK293T cells, either untreated or after infected with virus for knockdown of PRMT1 or MDN1 or empty vector control, were transfected with overexpression plasmid using PEI when cells grew to 70 to 80% confluency. Forty-eight hours later, cells were collected for biochemical assays.

Co-IP, mass spectrometry, and functional annotation analysis

Co-IP was performed using a conventional method as described (23). Cells were harvested, washed twice with cold PBS, and resuspended in lysis buffer (300 mM NaCl, 1% NP-40, 2 mM EDTA, 50 mM Tris-Cl pH7.5, and protease inhibitor cocktail). After 20 min on ice, cells were centrifuged for 20 min at 12,000 rpm. The supernatant was collected for immunoprecipitation using the antibody against IgG, an endogenous protein, or an HA- or MT-tag, which was linked to protein G sepharose beads. After incubation overnight at 4 °C, beads were washed in TBST buffer (25 mM Tris-Cl PH7.2, 150 mM NaCl, 0.5% Tween-20). Immuno-complexes were eluted by incubating the beads in 1× loading buffer at 95 °C and assayed with SDS-PAGE.

To identify PRMT1 interaction proteins with mass spectrometry, Co-IP was carried out in the same way above using NE-4C and HepG2 cells and an anti-PRMT1/Prmt1 antibody (Cell Signaling Technology, #2449). The immuno-precipitated protein complex for each bait and its corresponding negative control were concentrated by SDS-PGAE followed by Coomassie blue staining. The concentrated protein complex was excised as one single gel band and subjected to in-gel digestion. For in-gel protein digestion, cysteine residues were reduced by addition of 25 mM final of dithiothreitol (DTT) for 60 min at 70 °C and alkylated by addition of iodoacetamide at a final concentration of 90 mM for 30 min at room temperature in the dark. The proteins were then digested overnight at 37 °C with 0.2 μg of modified sequencing grade trypsin (Promega) in 50 mM ammonium bicarbonate. The resulting peptides were extracted from the gel by incubation in 50 mM ammonium bicarbonate: acetonitrile (1:1) for three times of 15 min at 37 °C, and then dried and resuspended with 10 μl of 3% acetonitrile, 2% FA before being subjected to LC-MS/MS analysis. The obtained peptides were analyzed by a nanoLC.2D (Eksigent Technologies) coupled with a Triple-TOF 5600+ System (AB SCIEX) as previously described (62).

For database searching, the original files were submitted to ProteinPilot Software (version 4.5, AB Sciex) for data analysis. LC-MS/MS data were searched against *Mus musculus* UniProt database (April 9, 2016, containing 50,943 sequences, http://www.uniprot.org/proteomes/UP000000589) or *Homo sapiens* UniProt database (April 9, 2016, containing 160,566 sequences, http://www.uniprot.org/proteomes/UP000005640). To identify proteins of interest, the mgf files were exported from ProteinPilot and subjected to Search Compare program in Protein Prospector (version 5.19.1, UCSF) for summarization, validation, and comparison of results. Parameters were set as previously described (62). Briefly, trypsin was set as the enzyme with a maximum of two missed cleavage sites. The mass tolerance was set at ±20 ppm for the parent ion, and a ±0.6 Da tolerance was set for the fragment ions. The expectation value cutoff that corresponds to a percent false positive (% FP) rate was determined by searching each project against a normal database concatenated with the reversed form of the database. The expectation values *versus* % FP rate for each search result were automatically plotted by an algorithm in Search Compare. Based on these results, an expectation value cutoff corresponding to ≤0.01% FP for all peptides was chosen. At this false positive rate, false protein hits from the decoy database were not observed.

According to the proteomics data, a protein is considered to be a putative PRMT1/Prmt1 interaction partner when at least two peptides of a protein are identified in the

immunoprecipitate with PRMT1/Prmt1 antibody but not in the precipitate with IgG antibody, or the fold change between the number of a protein peptide(s) in the sample precipitated by PRMT1/Prmt1 antibody and by IgG antibody is ≥3 (Tables S1 and S2). The mass spectrometry proteomics data have been deposited to the ProteomeXchange Consortium *via* the PRIDE partner repository with the dataset identifier PXD026851.

Functional annotation for the genes of the putative PRMT1/Prmt1 binding proteins was performed using the DAVID annotation tools (63) with default settings.

Total RNA preparation and reverse transcriptase–quantitative polymerase chain reaction (RT-qPCR)

Total RNAs were extracted from cells or tumors with TRIzol. cDNAs were transcribed from the total RNAs with the HiScript II first Strand cDNA Synthesis Kit (+gDNA wiper) (Vazyme, #R212-01/02), which contains the reagent for cleaning up the contamination of genomic DNA. qPCR was performed on a LightCycler 96 system (Roche) using the following parameters: one cycle of predenaturation at 95 °C for 5 min, followed by 40 cycles of denaturation at 95 °C for 10 s, annealing and extension at 60 °C for 30 s, and an additional cycle for melting curve. *β-Act/β-ACT* was detected as a loading control. Significance of changes in transcription was calculated based on experiments in triplicate using unpaired Student's *t* test. Data were presented as histograms with relative units of transcription levels. Primers for RT-qPCR are listed in Table S3.

Gene expression profiling assay on A549 cells with knockdown of PRMT1

A549 cells were infected with lentivirus carrying the empty vector (shCtrl) or carrying shPRMT1, respectively, and selected with puromycin. After significant phenotypic change occurred in cells with infection of shPRMT1 virus, both control and knockdown cells were collected and subjected to gene expression microarray. RNA extraction/purification, cRNA probe synthesis, probe hybridization to microarrays, signal processing, raw data analysis, and the subsequent enrichment and annotation of pathway and gene ontology were as exactly described (24). Results are shown as bar charts. Raw data are deposited in GEO under accession number GSE162840.

Mouse embryonic cortical cell isolation

All animal use in the research was approved by and in accordance with the guidelines of the Institutional Animal Care and Use Committee (IACUC) at the Model Animal Research Center of the Medical School, Nanjing University. For isolation of embryonic cortical cells, mouse embryos at E13.5 and E15.5 were resected and brains were excised from embryos. Cortical tissues were separated after removal of meninges and the ganglionic eminences. Cortical tissues were washed and homogenized in cold RIPA lysis buffer (20 mM Tris-HCl, pH 7.4, 150 mM NaCl, 1 mM EDTA, 1% NP-40, 0.5% sodium deoxycholate, and 0.1% SDS) supplemented with protease inhibitors (Roche, #04693132001). Lysates were cleared by centrifugation (14,000 rpm for 15 min) and subjected to immunoblotting.

Cell migration/invasion assays

Cell migration assay was performed in 24-well transwell plates with inserts of 8-μm pore size (Corning, #3422). Each 1×10^5 cells were suspended in 200 μl of serum-free culture medium, and added to the upper compartment. 500 μl of culture medium containing 10% FBS was added in the lower compartment. Plates were incubated at 37 °C for a desired time period, as indicated in the text. Afterward, cells were fixed with 37% formaldehyde, stained with 0.5% crystal violet for 10 min. Cells that did not migrate were removed. Migrated cells were washed with PBS and photographed.

For cell invasion assay, each 80 μl of Matrigel (Corning, #354234) was diluted in PBS (1:8) and distributed uniformly onto a 24-well transwell insert. 2×10^5 A549 or NE-4C cells or 5×10^5 A375 cells were added to Matrigel. Plates were incubated at 37 °C for desired time periods as indicated in the text. Afterward, cells were processed in the same way as in the migration assay.

Soft agar colony formation assay

The top and bottom layers of agar were 0.35% and 0.7%, respectively, of low melting agarose (BBI, #AB0015). Each 3000 cells were distributed in a well of a 6-well culture plate and cultured for desired time periods, as indicated in the text. Each experiment was performed in triplicate. Significance of difference in colony formation was calculated using unpaired Student's *t* test.

Chromatin immunoprecipitation (ChIP)

A375 cells were infected with lentivirus derived from empty vector or virus derived from PRMT1 knockdown vector. ChIP and subsequent qPCR were performed exactly as described (23). Antibodies used for ChIP were EZH2 (Cell Signaling Technology, #5246), H3K27me3 (Cell Signaling Technology, #9733) and H3K4me3 (Cell Signaling Technology, #9727). Significance in changes of precipitated chromatin by an antibody was calculated using unpaired Student's *t* test based on experiments in triplicate. Data are presented as histograms with relative units. Primers for qPCR are listed in Table S3.

Xenograft tumor assay

Immunodeficient nude Foxn1^{nu} mice with an age of 5 to 6 weeks were purchased from the National Resource Center for Mutant Mice and maintained in a specific-pathogen-free facility. A375 or NE-4C cells infected with control lentivirus or with knockdown virus were selected with puromycin. 3×10^6 A375 or 1×10^6 NE-4C cells, either control or knockdown, were suspended in 100 μl of sterile PBS, and injected subcutaneously into the dorsal flank of a mouse, respectively. Tumor growth was measured periodically, as indicated in the text. At the end of tumor growth, mice were sacrificed. Tumor tissues were excised and weighed. Tumor volume was calculated

using the formula: length × width^2/2. Significance of difference in tumor volumes between control and knockdown groups was calculated using two-way ANOVA followed by Bonferroni/Dunn (ANOVA-Bonferroni/Dunn) tests. Significance of difference in tumor weight was calculated with unpaired Student's *t* test.

Data availability

Proteomics data are available *via* ProteomeXchange with identifier PXD026851 (http://www.ebi.ac.uk/pride). Transcriptomics data are deposited in GEO under accession number GSE162840 (https://www.ncbi.nlm.nih.gov/geo/query/acc.cgi?acc=GSE162840).

Supporting information—This article contains supporting information (24, 35–37, 64–66).

Author contributions—Y. C. conceptualization; L. C., M. Z., and Y. C. formal analysis; Y. C. funding acquisition; L. C., M. Z., L. F., X. Y., N. C., L. X., and L. S. investigation; L. C., M. Z., and L. F. methodology; Y. C. project administration; Y. C. supervision; Y. C. writing – original draft.

Funding and additional information—This work was supported by Shenzhen Science and Technology Program, Shenzhen, China (Grant No.: JCYJ20210324120205015), and National Science Foundation of China (Grant No.: 31671499) to Y. C.

Conflicts of interest—The authors declare that they have no conflicts of interest with the contents of this article.

Abbreviations—The abbreviations used are: ChIP, chromatin immunoprecipitation; IF, immunofluorescence; MDN1, Midasin; mESC, mouse embryonic stem cell; NPC, neural progenitor cell; NSC, neural stem cell; PEI, polyethylenimine; primNSC, primitive neural stem cell; PRMT, protein arginine methyltransferase; RA, retinoic acid; RT-qPCR, reverse transcriptase–quantitative polymerase chain reaction; rRNA, ribosomal RNA; WCL, whole cell lysate.

References

1. de la Cruz, J., Karbstein, K., and Woolford, J. L., Jr. (2015) Functions of ribosomal proteins in assembly of eukaryotic ribosomes *in vivo*. *Annu. Rev. Biochem.* **84**, 93–129
2. Pelletier, J., Thomas, G., and Volarević, S. (2018) Ribosome biogenesis in cancer: New players and therapeutic avenues. *Nat. Rev. Cancer* **18**, 51–63
3. Konikkat, S., and Woolford, J. L., Jr. (2017) Principles of 60S ribosomal subunit assembly emerging from recent studies in yeast. *Biochem. J.* **474**, 195–214
4. Kressler, D., Hurt, E., Bergler, H., and Bassler, J. (2012) The power of AAA-ATPases on the road of pre-60S ribosome maturation-molecular machines that strip pre-ribosomal particles. *Biochim. Biophys. Acta* **1823**, 92–100
5. Baserga, R. (2007) Is cell size important? *Cell Cycle* **6**, 814–816
6. Turi, Z., Lacey, M., Mistrik, M., and Moudry, P. (2019) Impaired ribosome biogenesis: Mechanisms and relevance to cancer and aging. *Aging (Albany NY)* **11**, 2512–2540
7. Watanabe-Susaki, K., Takada, H., Enomoto, K., Miwata, K., Ishimine, H., Intoh, A., Ohtaka, M., Nakanishi, M., Sugino, H., Asashima, M., and Kurisaki, A. (2014) Biosynthesis of ribosomal RNA in nucleoli regulates pluripotency and differentiation ability of pluripotent stem cells. *Stem Cells* **32**, 3099–3111
8. Ito, N., Katoh, K., Kushige, H., Saito, Y., Umemoto, T., Matsuzaki, Y., Kiyonari, H., Kobayashi, D., Soga, M., Era, T., Araki, N., Furuta, Y., Suda, T., Kida, Y., and Ohta, K. (2018) Ribosome incorporation into somatic cells promotes lineage transdifferentiation towards multipotency. *Sci. Rep.* **8**, 1634
9. Ito, N., Anam, M. B., Ahmad, S. A. I., and Ohta, K. (2018) Transdifferentiation of human somatic cells by ribosome. *Dev. Growth Differ.* **60**, 241–247
10. Konstantinova, I. M., Tsimokha, A. S., and Mittenberg, A. G. (2008) Role of proteasomes in cellular regulation. *Int. Rev. Cell Mol. Biol.* **267**, 59–124
11. Bedford, L., Paine, S., Sheppard, P. W., Mayer, R. J., and Roelofs, J. (2010) Assembly, structure, and function of the 26S proteasome. *Trends Cell Biol.* **20**, 391–401
12. Schröter, F., and Adjaye, J. (2014) The proteasome complex and the maintenance of pluripotency: Sustain the fate by mopping up? *Stem Cell Res. Ther.* **5**, 24
13. Rousseau, A., and Bertolotti, A. (2018) Regulation of proteasome assembly and activity in health and disease. *Nat. Rev. Mol. Cell Biol.* **19**, 697–712
14. Lee, H. J., Gutierrez-Garcia, R., and Vilchez, D. (2017) Embryonic stem cells: A novel paradigm to study proteostasis? *FEBS J.* **284**, 391–398
15. Zhao, Y., Liu, X., He, Z., Niu, X., Shi, W., Ding, J. M., Zhang, L., Yuan, T., Li, A., Yang, W., and Lu, L. (2016) Essential role of proteasomes in maintaining self-renewal in neural progenitor cells. *Sci. Rep.* **6**, 19752
16. Blanc, R. S., and Richard, S. (2017) Arginine methylation: The coming of age. *Mol. Cell* **65**, 8–24
17. Yang, Y., and Bedford, M. T. (2013) Protein arginine methyltransferases and cancer. *Nat. Rev. Cancer* **13**, 37–50
18. Pawlak, M. R., Scherer, C. A., Chen, J., Roshon, M. J., and Ruley, H. E. (2000) Arginine N-methyltransferase 1 is required for early postimplantation mouse development, but cells deficient in the enzyme are viable. *Mol. Cell. Biol.* **20**, 4859–4869
19. Hsieh, J., Nakashima, K., Kuwabara, T., Mejia, E., and Gage, F. H. (2004) Histone deacetylase inhibition-mediated neuronal differentiation of multipotent adult neural progenitor cells. *Proc. Natl. Acad. Sci. U. S. A.* **101**, 16659–16664
20. Cho, Y., and Cavalli, V. (2014) HDAC signaling in neuronal development and axon regeneration. *Curr. Opin. Neurobiol.* **27**, 118–126
21. Han, X., Gui, B., Xiong, C., Zhao, L., Liang, J., Sun, L., Yang, X., Yu, W., Si, W., Yan, R., Yi, X., Zhang, D., Li, W., Li, L., Yang, J., *et al.* (2014) Destabilizing LSD1 by Jade-2 promotes neurogenesis: An antibraking system in neural development. *Mol. Cell* **55**, 482–494
22. Sáez, J. E., Gómez, A. V., Barrios, Á. P., Parada, G. E., Galdames, L., González, M., and Andrés, M. E. (2015) Decreased expression of CoREST1 and CoREST2 together with LSD1 and HDAC1/2 during neuronal differentiation. *PLoS One* **10**, e0131760
23. Lei, A., Chen, L., Zhang, M., Yang, X., Xu, L., Cao, N., Zhang, Z., and Cao, Y. (2019) EZH2 regulates protein stability *via* recruiting USP7 to mediate neuronal gene expression in cancer cells. *Front. Genet.* **10**, 422
24. Zhang, Z., Lei, A., Xu, L., Chen, L., Chen, Y., Zhang, X., Gao, Y., Yang, X., Zhang, M., and Cao, Y. (2017) Similarity in gene-regulatory networks suggests that cancer cells share characteristics of embryonic neural cells. *J. Biol. Chem.* **292**, 12842–12859
25. Cao, Y. (2017) Tumorigenesis as a process of gradual loss of original cell identity and gain of properties of neural precursor/progenitor cells. *Cell Biosci.* **7**, 61
26. Xu, L., Zhang, M., Shi, L., Yang, X., Chen, L., Cao, N., Lei, A., and Cao, Y. (2021) Neural stemness contributes to cell tumorigenicity. *Cell Biosci.* **11**, 21
27. [preprint] Cao, Y. (2020) Neural is fundamental: Neural stemness as the ground state of cell tumorigenicity and differentiation potential. *Preprints*. https://doi.org/10.20944/preprints202012.0122.v1
28. Bustelo, X. R., and Dosil, M. (2018) Ribosome biogenesis and cancer: Basic and translational challenges. *Curr. Opin. Genet. Dev.* **48**, 22–29
29. Chen, Y., Zhang, Y., and Guo, X. (2017) Proteasome dysregulation in human cancer: Implications for clinical therapies. *Cancer Metastasis Rev.* **36**, 703–716

30. Mofers, A., Pellegrini, P., Linder, S., and D'Arcy, P. (2017) Proteasome-associated deubiquitinases and cancer. *Cancer Metastasis Rev.* **36**, 635–653
31. Soave, C. L., Guerin, T., Liu, J., and Dou, Q. P. (2017) Targeting the ubiquitin-proteasome system for cancer treatment: Discovering novel inhibitors from nature and drug repurposing. *Cancer Metastasis Rev.* **36**, 717–736
32. Baldwin, R. M., Morettin, A., and Côté, J. (2014) Role of PRMTs in cancer: Could minor isoforms be leaving a mark? *World J. Biol. Chem.* **5**, 115–129
33. Bennett, R. L., and Licht, J. D. (2018) Targeting epigenetics in cancer. *Annu. Rev. Pharmacol. Toxicol.* **58**, 187–207
34. Mohammad, H. P., Barbash, O., and Creasy, C. L. (2019) Targeting epigenetic modifications in cancer therapy: Erasing the roadmap to cancer. *Nat. Med.* **25**, 403–418
35. Robson, A., Owens, N. D., Baserga, S. J., Khokha, M. K., and Griffin, J. N. (2016) Expression of ribosomopathy genes during Xenopus tropicalis embryogenesis. *BMC Dev. Biol.* **16**, 38
36. Hasegawa, K., Shiraishi, T., and Kinoshita, T. (1999) Xoom: A novel oocyte membrane protein maternally expressed and involved in the gastrulation movement of Xenopus embryos. *Int. J. Dev. Biol.* **43**, 479–485
37. Hu, R., Huang, W., Liu, J., Jin, M., Wu, Y., Li, J., Wang, J., Yu, Z., Wang, H., and Cao, Y. (2019) Mutagenesis of putative ciliary genes with the CRISPR/Cas9 system in zebrafish identifies genes required for retinal development. *FASEB J.* **33**, 5248–5256
38. Cheung, N., Chan, L. C., Thompson, A., Cleary, M. L., and So, C. W. (2007) Protein arginine-methyltransferase-dependent oncogenesis. *Nat. Cell Biol.* **9**, 1208–1215
39. Mathioudaki, K., Papadokostopoulou, A., Scorilas, A., Xynopoulos, D., Agnanti, N., and Talieri, M. (2008) The PRMT1 gene expression pattern in colon cancer. *Br. J. Cancer* **99**, 2094–2099
40. Yoshimatsu, M., Toyokawa, G., Hayami, S., Unoki, M., Tsunoda, T., Field, H. I., Kelly, J. D., Neal, D. E., Maehara, Y., Ponder, B. A., Nakamura, Y., and Hamamoto, R. (2011) Dysregulation of PRMT1 and PRMT6, type I arginine methyltransferases, is involved in various types of human cancers. *Int. J. Cancer* **128**, 562–573
41. Choucair, A., Pham, T. H., Omarjee, S., Jacquemetton, J., Kassem, L., Trédan, O., Rambaud, J., Marangoni, E., Corbo, L., Treilleux, I., and Le Romancer, M. (2019) The arginine methyltransferase PRMT1 regulates IGF-1 signaling in breast cancer. *Oncogene* **38**, 4015–4027
42. Song, C., Chen, T., He, L., Ma, N., Li, J. A., Rong, Y. F., Fang, Y., Liu, M., Xie, D., and Lou, W. (2020) PRMT1 promotes pancreatic cancer growth and predicts poor prognosis. *Cell Oncol.* **43**, 51–62
43. He, L., Hu, Z., Sun, Y., Zhang, M., Zhu, H., Jiang, L., Zhang, Q., Mu, D., Zhang, J., Gu, L., Yang, Y., Pan, F. Y., Jia, S., and Guo, Z. (2020) PRMT1 is critical to FEN1 expression and drug resistance in lung cancer cells. *DNA Repair (Amst.)* **95**, 102953
44. Yin, X. K., Wang, Y. L., Wang, F., Feng, W. X., Bai, S. M., Zhao, W. W., Feng, L. L., Wei, M. B., Qin, C. L., Wang, F., Chen, Z. L., Yi, H. J., Huang, Y., Xie, P. Y., Kim, T., *et al.* (2021) PRMT1 enhances oncogenic arginine methylation of NONO in colorectal cancer. *Oncogene* **40**, 1375–1389
45. Chau, K. F., Shannon, M. L., Fame, R. M., Fonseca, E., Mullan, H., Johnson, M. B., Sendamarai, A. K., Springel, M. W., Laurent, B., and Lehtinen, M. K. (2018) Downregulation of ribosome biogenesis during early forebrain development. *Elife* **7**, e36998
46. Weintraub, H., Tapscott, S. J., Davis, R. L., Thayer, M. J., Adam, M. A., Lassar, A. B., and Miller, A. D. (1989) Activation of muscle-specific genes in pigment, nerve, fat, liver, and fibroblast cell lines by forced expression of MyoD. *Proc. Natl. Acad. Sci. U. S. A.* **86**, 5434–5438
47. Raman, N., Weir, E., and Müller, S. (2016) The AAA ATPase MDN1 acts as a SUMO-targeted regulator in mammalian pre-ribosome remodeling. *Mol. Cell* **64**, 607–615
48. Clarke, D. L., Johansson, C. B., Wilbertz, J., Veress, B., Nilsson, E., Karlström, H., Lendahl, U., and Frisén, J. (2000) Generalized potential of adult neural stem cells. *Science* **288**, 1660–1663
49. Tropepe, V., Hitoshi, S., Sirard, C., Mak, T. W., Rossant, J., and van der Kooy, D. (2001) Direct neural fate specification from embryonic stem cells: A primitive mammalian neural stem cell stage acquired through a default mechanism. *Neuron* **30**, 65–78
50. Muñoz-Sanjuán, I., and Brivanlou, A. H. (2002) Neural induction, the default model and embryonic stem cells. *Nat. Rev. Neurosci.* **3**, 271–280
51. Smukler, S. R., Runciman, S. B., Xu, S., and van der Kooy, D. (2006) Embryonic stem cells assume a primitive neural stem cell fate in the absence of extrinsic influences. *J. Cell Biol.* **172**, 79–90
52. Gilbert, S. F., and Barresi, M. J. (2016) Early amphibian development. In *Developmental Biology*, 11th Ed, Sinauer Associates, Inc, Sunderland, MA: 333–364
53. Huang, Z., Wu, Q., Guryanova, O. A., Cheng, L., Shou, W., Rich, J. N., and Bao, S. (2011) Deubiquitylase HAUSP stabilizes REST and promotes maintenance of neural progenitor cells. *Nat. Cell Biol.* **13**, 142–152
54. Chern, M. K., Chang, K. N., Liu, L. F., Tam, T. C., Liu, Y. C., Liang, Y. L., and Tam, M. F. (2002) Yeast ribosomal protein L12 is a substrate of protein-arginine methyltransferase 2. *J. Biol. Chem.* **277**, 15345–15353
55. Bachand, F., and Silver, P. A. (2004) PRMT3 is a ribosomal protein methyltransferase that affects the cellular levels of ribosomal subunits. *EMBO J.* **23**, 2641–2650
56. Swiercz, R., Person, M. D., and Bedford, M. T. (2005) Ribosomal protein S2 is a substrate for mammalian PRMT3 (protein arginine methyltransferase 3). *Biochem. J.* **386**, 85–91
57. Shin, H. S., Jang, C. Y., Kim, H. D., Kim, T. S., Kim, S., and Kim, J. (2009) Arginine methylation of ribosomal protein S3 affects ribosome assembly. *Biochem. Biophys. Res. Commun.* **385**, 273–278
58. Ren, J., Wang, Y., Liang, Y., Zhang, Y., Bao, S., and Xu, Z. (2010) Methylation of ribosomal protein S10 by protein-arginine methyltransferase 5 regulates ribosome biogenesis. *J. Biol. Chem.* **285**, 12695–12705
59. Hsu, J. H., Hubbell-Engler, B., Adelmant, G., Huang, J., Joyce, C. E., Vazquez, F., Weir, B. A., Montgomery, P., Tsherniak, A., Giacomelli, A. O., Perry, J. A., Trowbridge, J., Fujiwara, Y., Cowley, G. S., Xie, H., *et al.* (2017) PRMT1-mediated translation regulation is a crucial vulnerability of cancer. *Cancer Res.* **77**, 4613–4625
60. Zhang, L., Tran, N. T., Su, H., Wang, R., Lu, Y., Tang, H., Aoyagi, S., Guo, A., Khodadadi-Jamayran, A., Zhou, D., Qian, K., Hricik, T., Côté, J., Han, X., Zhou, W., *et al.* (2015) Cross-talk between PRMT1-mediated methylation and ubiquitylation on RBM15 controls RNA splicing. *Elife* **4**, e07938
61. Fong, J. Y., Pignata, L., Goy, P. A., Kawabata, K. C., Lee, S. C., Koh, C. M., Musiani, D., Massignani, E., Kotini, A. G., Penson, A., Wun, C. M., Shen, Y., Schwarz, M., Low, D. H., Rialdi, A., *et al.* (2019) Therapeutic targeting of RNA splicing catalysis through inhibition of protein arginine methylation. *Cancer Cell* **36**, 194–209.e9
62. Zhang, J., Zhao, R., Yu, C., Bryant, C. L. N., Wu, K., Liu, Z., Ding, Y., Zhao, Y., Xue, B., Pan, Z. Q., Li, C., Huang, L., and Fang, L. (2020) IKK-mediated regulation of the COP9 signalosome *via* phosphorylation of CSN5. *J. Proteome Res.* **19**, 1119–1130
63. Huang, D. W., Sherman, B. T., Tan, Q., Kir, J., Liu, D., Bryant, D., Guo, Y., Stephens, R., Baseler, M. W., Lane, H. C., and Lempicki, R. A. (2007) DAVID bioinformatics resources: Expanded annotation database and novel algorithms to better extract biology from large gene lists. *Nucleic Acids Res.* **35**, W169–W175
64. Griffin, J. N., Sondalle, S. B., Robson, A., Mis, E. K., Griffin, G., Kulkarni, S. S., Deniz, E., Baserga, S. J., and Khokha, M. K. (2018) RPSA, a candidate gene for isolated congenital asplenia, is required for pre-rRNA processing and spleen formation in Xenopus. *Development* **145**, dev166181
65. Scholnick, J., Sinor, C., Oakes, J., Outten, W., and Saha, M. (1997) Differential expression of Xenopus ribosomal protein gene XlrpS1c. *Biochim. Biophys. Acta* **1354**, 72–82
66. Vernon, A. E., and Philpott, A. (2003) The developmental expression of cell cycle regulators in Xenopus laevis. *Gene Expr. Patterns* **3**, 179–192